Rotating Propeller Solitons

Tal Carmon, Raam Uzdin, Claude Pigier, Ziad H. Musslimani, Mordechai Segev, and A. Nepomnyashchy

Technion-Israel Institute of Technology, Haifa 32000, Israel
(Received 22 September 2000; published 17 September 2001)

We demonstrate experimentally and theoretically (both analytically and numerically) a new type of spatial soliton: a rotating "propeller" soliton. This is a composite soliton made of a *rotating* dipole component jointly trapped with a bell-shaped component. We observe as much as 239° of rotation over 13 mm of propagation (6.5 diffraction lengths).

Self-trapping of an optical beam occurs when the beam induces, through a nonlinearity, a waveguide structure and, at the same time, is guided in its own induced waveguide [1]. Such beams are commonly referred to as spatial solitons [2]. The simplest (so-called scalar) soliton occurs when the soliton constitutes a single field, which populates the lowest mode of its own induced waveguide. A more complex soliton, a vector soliton, occurs when more than one field populates the lowest waveguide mode. These were first suggested by Manakov [3] in Kerr media, when the self- and the cross-phase modulations are equal. Manakov-like solitons were recently observed experimentally [4]. Moreover, solitons can also be composite: They can constitute optical fields that populate *different* modes of their jointly induced waveguide. In their simplest realization, composite solitons are made of a bell-shaped (bright) component populating the lowest mode and a dark component being the second mode [5,6]. A more interesting situation occurs when the field constituents of the composite soliton populate different bound modes of their jointly induced potential as suggested for temporal [7], as well as spatial [8], solitons. These multimode solitons, first observed in [9], offer many new features, e.g., shape transformation [10]. All of these studies refer to $(1 + 1)$D solitons which trap in a single transverse dimension.

Composite solitons in $(2 + 1)$D (which self-trap in both transverse dimensions) were proposed only recently: first in a vortex-type form [11], in which one component is bell shaped and the other is a ring carrying topological charge, and second in a dipole form, where the second component is a 2D dipole [12]. Experimental observations of $(2 + 1)$D dipole-type composite solitons followed soon thereafter [13]. The possibility of realizing $(2 + 1)$D composite solitons experimentally offers many new features, e.g., in their interaction [14] and stability [15] properties. Such solitons also directly relate to two-component Bose-Einstein condensates (BEC) [16], described by similar equations. In the BEC case, the components correspond to hyperfine states of the cooled atomic gas in a spherical trap, and resemble vortex-type composite solitons [11]. It is already obvious that the interactions between composite solitons, especially those that carry angular momentum, whether in the optical or atomic domains, offer unique properties.

Here we present a new type of composite soliton: a *rotating* dipole soliton. The intensity structure of the soliton constituents rotates throughout propagation. In particular, the dipole mode has a double-helix structure, and its equal-phase planes resemble propeller blades [Fig. 1(a)]. Hence, we name it a "propeller soliton." *This is the first soliton whose intensity structure (not only its phase) rotates during propagation.* The dimensionless equations for the slowly varying envelopes, Ψ_1 and Ψ_2, are

$$i(\partial \Psi_{1,2}/\partial \zeta) + \nabla_\perp^2 \Psi_{1,2} + \Delta n(I)\Psi_{1,2} = 0, \quad (1)$$

where ζ is the propagation distance, $\nabla_\perp^2 = \partial^2/\partial \xi^2 + \partial^2/\partial \eta^2$, $\Delta n(I) = -1/(1 + I)$ is the refractive-index change, and $I = |\Psi_1|^2 + |\Psi_2|^2$ is the total intensity. This choice of Δn corresponds to propagation in a homogeneously broadened electronic two-level system, and is also a reasonable approximation of the photorefractive
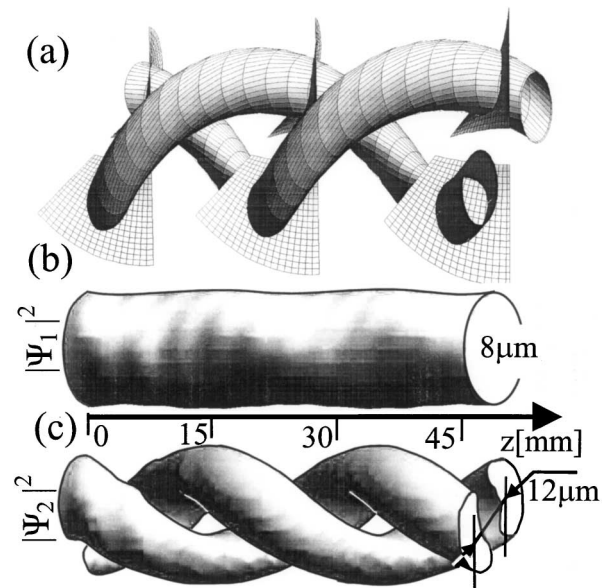

FIG. 1. (a) Illustration of the rotating-dipole mode of a propeller soliton. The propeller-blade surfaces represent the equal-phase surfaces. (b),(c) *Calculated* dynamics of the fundamental and dipole modes of a propeller soliton. Shown are the modal intensities for $|\Psi_1(\rho = 0)|^2 = 4$ and $|\Psi_2|^2_{\text{peak}} = 0.45$, in units of the saturation intensity. The slightly elliptic, 8 μm FWHM, fundamental mode (b) rotates in unison with a 12 μm peak-to-peak dipole (c).

screening nonlinearity. The nonlinearity must be saturable, otherwise, e.g., in Kerr media, such 2D beams undergo catastrophic collapse. We emphasize that propeller-type composite solitons should exist in *any* saturable nonlinearity in a conservative (loss-free) system. Interference terms (e.g., $\Psi_1\Psi_2^*$) should not contribute to Δn, so the induced waveguide does not vary during propagation. There are several methods of eliminating the contribution of such terms to Δn [2,13]. We employ the method in which Ψ_1 and Ψ_2 are mutually incoherent, so the phase of $\Psi_1\Psi_2^*$ terms varies randomly in time much faster than the nonlinearity can respond, and their contribution to Δn averages out [17]. We seek self-trapped solutions, including those rotating about ζ, in the form

$$\Psi_{1,2}(\rho,\theta,\zeta) = \psi_{1,2}(\rho,\theta,\zeta)\exp(i\mu_{1,2}\zeta), \qquad (2)$$

where $\mu_{1,2}$ are the (real) propagation constants. The first, and simplest, solution is the radially symmetric, scalar (stationary in ζ) soliton, for which $\psi_1 = u_1(\rho)$ and $\psi_2 = 0$. A second case is the vortex-type composite soliton [11,14] for which $\psi_1 = u_1(\rho)$ and $\psi_2 = u_2(\rho)\exp(im\theta)$, where m (integer) is the topological charge. A third case is the dipole-type composite soliton [12] $\psi_1 = u_1(\rho,\theta)$ and $\psi_2 = u_2(\rho,\theta)$. For all of these three cases, the intensity structure is *stationary* in ζ. Here we are interested in a new case: *dipole solitons that rotate about ζ* (propeller-type composite solitons). Thus, neither ψ_1 nor ψ_2 have radial symmetry, and their intensity structure rotates while propagating.

Deriving the solutions for the rotating propeller soliton, we first present a *weakly nonlinear* analysis of the problem. It can be shown that this new class of solutions [in the form of Eq. (2)] appears through a *bifurcation* (in parameter space) from the family of radially symmetric scalar solutions. Near the bifurcation point, ψ_1 and ψ_2 can be expanded as $\psi_1(\rho,\theta,Z) = \psi_1^{(0)} + \varepsilon^2\psi_1^{(2)} + \ldots$ and $\psi_2(\rho,\theta,Z) = \varepsilon\psi_2^{(1)} + \varepsilon^3\psi_2^{(3)} + \ldots$, respectively, and the characteristic scale for the longitudinal coordinate is $Z = \varepsilon^2\zeta$. Here, $\psi_1^{(0)} = u_1(\rho)$ is radially symmetric, and $\psi_2^{(1)}(\rho,\theta,Z)$ satisfies the linear eigenvalue problem

$$\nabla_\perp^2\psi_2^{(1)} - \mu_2\psi_2^{(1)} + \Delta n(|u_1(\rho)|^2)\psi_2^{(1)} = 0 \qquad (3)$$

with the solution $\psi_2^{(1)} = u_2(\rho)[C_+(Z)\exp(i\theta) + C_-(Z)\exp(-i\theta)]$, where $C_\pm(Z)$ *cannot be determined in the framework of a linear theory*. The asymptotic weakly nonlinear theory, which takes into account the second order correction $\psi_1^{(2)}(\rho,\theta,Z)$, provides closed amplitude equations $idC_\pm/dZ = -C_\pm(a|C_\pm|^2 + b|C_\mp|^2)$, where a and b are constants calculated from the solvability condition in the third order in ε. Defining $C_\pm(Z) = R_\pm\exp(i\phi_\pm)$ yields $\partial\phi_\pm/\partial Z = (aR_\pm^2 + bR_\mp^2) \equiv \Omega_\pm$, where $R_\pm$ and $\Omega_\pm$ are real constants. Hence, $C_\pm(Z) = R_\pm\exp(i\Omega_\pm Z)$ and

$$\psi_2^{(1)} = u_2(\rho)[R_+\exp i(\Omega_+ Z + \theta)$$
$$+ R_-\exp i(\Omega_- Z - \theta)]. \qquad (4)$$

This family of solutions includes the vortex-type composite soliton [11,14], $\psi_2^{(1)} = u_2(\rho)[R_+\exp i(\Omega_+ Z + \theta)]$ (re-

covered for $R_- = 0$), whose phase rotates, but whose intensity structure, $|\psi_2^{(1)}|^2$, has radial symmetry and displays no rotation. Another member of this family is the nonrotating dipole-type composite soliton [12], $\psi_2^{(1)} = u_2(\rho) \times [R\exp i(\Omega Z)\cos(\theta)]$, recovered when $R_\pm = R/2$, $\Omega_\pm = \Omega$. This radially asymmetric dipole does not rotate, not even in its phase. Except for these particular cases, all other solutions described by Eq. (4) are new solutions having both their intensity structure and their phase rotating during propagation. These are the propeller-type solutions. The rotation rates of the intensity and the phase are different: The intensity, $|\psi_2^{(1)}|^2 = u_2^2(\rho)\{R_+^2 + R_-^2 + 2R_+R_- \times \cos[(\Omega_+ - \Omega_-)Z + 2\theta]\}$, rotates with an angular velocity $(\Omega_- - \Omega_+)/2$, whereas the phase of $\psi_2^{(1)}$ rotates with a *different* angular velocity. The rotation direction is determined by which is larger, R_+ or R_-. The Poynting vector forms a helix during propagation, because the energy flow is in a direction perpendicular to the equal-phase planes [Fig. 1(a)]. *Because the rotation rates of the intensity and the phase are different, there are no stationary solutions in any rotating frame.* One cannot simply generalize the stationary-dipole composite solitons found earlier [12] and obtain the propeller solitons by transforming the equations into a rotating frame. Propeller solitons are new creatures and can be considered as more general than the stationary vortex- and dipole-type composite solitons [11,12].

To find a propeller-type composite soliton solution, one can choose the parameters determining the rotation rates rather freely (one can increase $|\psi_2|^2$ as long as $|\Omega_\pm| \ll |\mu_2|$) and use a 1D relaxation code to find $u_1(\rho)$, $u_2(\rho)$, μ_1, and μ_2 from Eq. (1) by replacing $\Psi_{1,2}$ by $u_{1,2}(\rho) \times \exp(i\mu_{1,2}\zeta)$. This procedure holds as long as $|\psi_1|^2 \gg |\psi_2|^2$. When the modal intensities are comparable, a 2D relaxation code should be used to find $\Psi_{1,2}(\rho,\theta,\zeta)$. To confirm and demonstrate the propeller-type soliton, we investigate the propagation of the solution given by Eq. (4), by launching this solution into the nonlinear medium described by Eq. (1), and observe the propagation dynamics using a standard $(2 + 1)$D beam propagation code for two coupled fields [14]. The results are shown (in dimensional units [18]) in Figs. 1(b) and 1(c) and display the propagation of a solution with $|\Psi_1|_{\text{peak}}^2$ nine times larger than the peak intensity of the dipole mode $|\Psi_2|_{\text{peak}}^2$. In this example, $R_+ = 0.9$, $R_- = 0.15$, displaying an 8 μm FWHM almost circular bell-shaped Ψ_1, and a rotating dipole-type Ψ_2 with a 12 μm separation between the "poles" of the dipole. The two modes ($\Psi_{1,2}$) rotate together, in a self-trapped fashion, with a rate of $\sim 9°$ per mm [18]. The propagation results [Figs. 1(b) and 1(c)] convincingly indicate that the solution of Eq. (4) is a good approximation, since both Ψ_1 and Ψ_2 exhibit stable self-trapped propagation and rotate in unison. In our simulations, we find that the *total* power of *each* field is conserved, and the linear and angular momenta of all fields *together* are conserved.

We emphasize that, although the solution of Eq. (4) is valid only within the weakly nonlinear regime, composite propeller solitons do exist in a larger range of parameters.

In fact, our simulation [Figs. 1(b) and 1(c)] shows that Ψ_1 has a slightly elliptic shape thus extending beyond the $|\Psi_1|^2 \gg |\Psi_2|^2$ regime.

Experimentally, we generate the propeller solitons in the photorefractive media, employing the screening nonlinearity [19], and the mutual incoherence method to observe multicomponent solitons [17]. We expand and collimate a 488 nm laser beam and split it into Ψ_1 and Ψ_2. The Ψ_2 beam is first passed through a helical phase mask, which multiplies the beam by $\exp(i\theta)$, providing the angular momentum necessary for rotation. Then, to shape it as a dipole, the plane of the mask is reproduced (with a $4f$ system) and a metal wire is introduced so that it crosses the beam from side-to-side through its center. The components are combined (with a beam splitter) after ensuring that the path difference between them exceeds the coherence length of the laser [9,13]. The combined structure is imaged onto the input face of the crystal, so that the input face is a demagnified image plane of the vortex crossed by the wire. This structure is propagating along the a axis of an $Sr_{0.6}Ba_{0.4}Nb_2O_6$ (SBN:60) crystal, in the standard configuration [20]. The crystal is also illuminated uniformly with a background beam (to tune the degree of saturation of the nonlinearity), which is polarized orthogonally to the Ψ_1, Ψ_2 beams. The background beam is made spatially incoherent (with a rotating diffuser), and remains uniform even when large fields are applied. The intensity distributions at the input and output faces are imaged on a CCD camera. The modes can be inspected individually by using the method described in [9,13].

We measure the rotation rate and propagation dynamics of the dipole mode at various distances, by launching the soliton in a series of samples of 1, 6, and 13 mm lengths, all of which being SBN:60 crystals of the same properties. *These samples have been verified to support solitons under the same parameters.* Figures 2(a)–2(d) show photographs of $|\Psi_2|^2$ for $m = -1$ at the crystal input and after propagating 1, 6, and 13 mm, respectively, when jointly trapped with $|\Psi_1|^2$ (not shown here), together forming a soliton. The dipole rotation rate vs propagation distance is shown in the graph (Fig. 2), displaying a rotation rate of 20° per mm, and a total rotation (for the 13-mm-long sample) of up to 239°. The discrepancy between this rate and the calculated rate (of Fig. 1) results from the fact that the calculation is conducted in the weakly nonlinear regime using a 1D relaxation code to find the wave functions. The approximation leads to rather slow rotation rates. Experimentally, we are motivated to display as much rotation effects as possible, even though at present we cannot simulate them. To properly simulate our experimental results, a two-dimensional relaxation code is necessary. We also expect the anisotropy of the photorefractive screening nonlinearity [21] to modify the rotation rate from that in a fully isotropic nonlinearity (as assumed in our model). To a large extent, the very fact that the propeller composite soliton survives (experimentally), in spite of the anisotropy, highlights its stability and robustness.
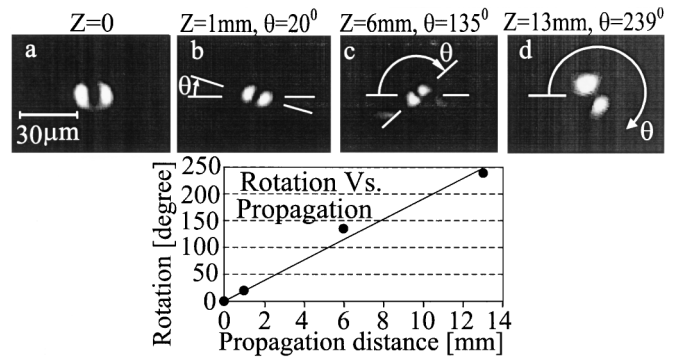
FIG. 2. Experimentally observed propagation of the dipole mode of a propeller soliton with $|\Psi_1|^2_{max} = 10$, $|\Psi_2|^2_{max} = 1$, and $m = -1$. (a) Input, with 13.5 μm separation between the dipole peaks. (b) Trapped $|\Psi_2|^2$ output after 1 mm propagation, displaying 20° rotation. (c) Trapped $|\Psi_2|^2$ output after 6 mm propagation, displaying 135° rotation. (d) Trapped $|\Psi_2|^2$ output after 13 mm propagation, displaying 239° rotation. The graph displays the rotation angle vs distance, extracted from (a) to (d), with a linear fit; the measurement errors are ± 0.05 mm for the propagation length and $\pm 3°$ for the rotation angle.

In order to prove that the angular momentum of the dipole is the reason for its rotation, we compare the rotation of identical composite solitons with opposite topological charges. The input fields [Figs. 3(a) and 3(f)], Ψ_1 and Ψ_2, are the same, except that the topological charge is reversed from $m = -1$ to $m = 1$. After 6 mm propagation, the former rotates 135° clockwise [Fig. 3(b)], whereas the latter rotates 142° counterclockwise [Fig. 3(c)].

We emphasize that the propeller soliton consists of two modes: The rotating dipole mode cannot self-trap all by it-
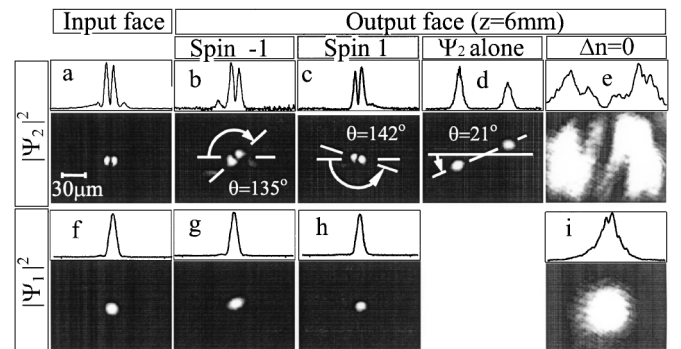

FIG. 3. Experimentally observed propagation of a propeller soliton with $|\Psi_1|^2_{max} = 10$, $|\Psi_2|^2_{max} = 1$ for 6 mm propagation (three diffraction lengths). (a),(f) Input intensities of the modes. The separation between the dipole peaks in (a) is 11 μm, and the FWHM of the fundamental mode in (f) is 11 μm. (b),(g) Self-trapped output with 3300 V/cm applied. The dipole mode rotates by 135° and its peak-to-peak separation is 13 μm. The fundamental mode is slightly elliptic. (c),(h) Same as (b),(g) with opposite spin $m = 1$. Inverting the topological charge leaves all dimensions and rotation angles similar to those of (b)-(g), but leads to rotation in the opposite direction. (d) Output dipole mode at 3300 V/cm when the fundamental mode is blocked. The dipole evolves into two solitons separated by a distance of 114 μm and overall rotation of 21°. (e),(i) Output intensities of the dipole mode and the fundamental mode when the nonlinearity is set to zero. Separation between peaks in (e) is 113 μm, and the FWHM of the fundamental mode in (i) is 48 μm.

self when the fundamental component is blocked. Instead, when we turn off the fundamental mode Ψ_1 and examine the propagating stand-alone dipole mode Ψ_2, the input dipole evolves into a pair of repelling $(2 + 1)$D solitons [Fig. 3(d)] with an output separation about 10 times larger than the distance between the poles of the composite propeller soliton [Fig. 3(c)]. Note that the input Ψ_2 has angular momentum, and thus the output Ψ_2 is rotated, but the rotation angle is small. This is because the angular momentum is conserved (as we indeed find in our numerical simulations). Thus, the rotation rate of the "repelling poles" of Fig. 3(d) decreases with the peak-to-peak separation distance squared (the "skater on the ice effect").

Finally, we examine the propagation of both modes (Ψ_1 and Ψ_2) in the absence of nonlinearity, that is, during linear diffraction. When we turn the nonlinearity off (by turning off the bias voltage), the beams diffract to the structures shown in Figs. 3(e) and 3(i) and the modes are no longer trapped. The beams expand considerably, and the separation between the dipole peaks increases by more than tenfold. This shows that the 6 mm propagation distance in our experiments is ≈ 3 diffraction lengths.

In conclusion, we have demonstrated propeller-type composite solitons: bimodal solitons that contain a rotating dipole. This idea can be extended to include rotating quadrupoles, hexapoles, etc. What makes propeller-type solitons so interesting is the fact that they display two different rotations: the rotation of their intensity structure (the double helix) and the rotation of their phase. To a large extent, propeller-type composite solitons resemble rotating molecules. This adds another feature to the analogy between solitons and particles, and the extension to multi-soliton systems, including collisions, seems promising. Finally, we point out the relevance to other systems that support two-component solitons, and specifically to two-component BECs [16]. For BECs, self-trapping occurs because of the balance between kinetic energy and repulsive atom-atom collisions. Two-component BECs form by trapping atoms at different electronic states [22]. Since dark solitons in BECs have already been observed experimentally [23], we envision that multicomponent solitons, in particular those that carry angular momentum, can be constructed with atoms. The phenomenon, however, of composite solitons carrying angular momentum is universal.

[1] G. A. Askar'yan, Sov. Phys. JETP **15**, 1088 (1962); A. W. Snyder, D. J. Mitchell, L. Poladian, and F. Landouceur, Opt. Lett. **16**, 21 (1991).

[2] G. Stegeman and M. Segev, Science **286**, 1518 (1999).

[3] S. V. Manakov, Sov. Phys. JETP **38**, 248 (1974).

[4] J. U. Kang *et al.,* Phys. Rev. Lett. **76**, 3699 (1996); Z. Chen, M. Segev, T. Coskun, and D. N. Christodoulides, Opt. Lett. **21**, 1436 (1996).

[5] D. N. Christodoulides, Phys. Lett. A **132**, 451 (1988); S. Trillo *et al.,* Opt. Lett. **13**, 871 (1988).

[6] M. Shalaby and A. J. Barthelemy, IEEE J. Quantum Electron. **28**, 2736 (1992); Z. Chen, M. Segev, T. Coskun, D. Christodoulides, Y. Kivshar, and V. Afanasjev, Opt. Lett. **21**, 1821 (1996).

[7] D. N. Christodoulides and R. I. Joseph, Opt. Lett. **13**, 53 (1988); M. V. Tratnik and J. E. Sipe, Phys. Rev. A **38**, 2001 (1988); M. Haelterman, A. P. Sheppard, and A. W. Snyder, Opt. Lett. **18**, 1406 (1993).

[8] A. W. Snyder, S. J. Hewlett, and D. J. Mitchell, Phys. Rev. Lett. **72**, 1012 (1994).

[9] M. Mitchell, M. Segev, and D. N. Christodoulides, Phys. Rev. Lett. **80**, 4657 (1998).

[10] N. Akhmediev, W. Krolikowski, and A. W. Snyder, Phys. Rev. Lett. **81**, 4632 (1998); W. Krolikowski *et al.,* Phys. Rev. E **59**, 4654 (1999).

[11] Z. H. Musslimani, M. Segev, D. N. Christodoulides, and M. Soljacic, Phys. Rev. Lett. **84**, 1164 (2000); Opt. Lett. **25**, 61 (2000).

[12] J. J. Garcia-Ripoll, V. M. Perez-Garcia, E. A. Ostrovskaya, and Y. S. Kivshar, Phys. Rev. Lett. **85**, 82 (2000).

[13] T. Carmon, C. Anastassiou, S. Lan, D. Kip, Z. Musslimani, M. Segev, and D. N. Christodoulides, Opt. Lett. **25**, 1113 (2000); W. Krolikowski, E. A. Ostrovskaya, C. Weilnau, M. Geisser, G. McCarthy, Y. S. Kivshar, C. Denz, and B. Luther-Davies, Phys. Rev. Lett. **85**, 1424 (2000).

[14] Z. H. Musslimani, M. Soljacic, M. Segev, and D. N. Christodoulides, Phys. Rev. Lett. **86**, 799 (2001); Phys. Rev. E **63**, 66608 (2001).

[15] J. M. Malmberg *et al.,* Opt. Lett. **25**, 643 (2000).

[16] M. R. Matthews *et al.,* Phys. Rev. Lett. **83**, 2498 (1999); J. J. Garcia-Ripoll and V. M. Perez-Garcia, *ibid.* **84**, 1424 (2000).

[17] D. N. Christodoulides *et al.,* Appl. Phys. Lett. **68**, 1763 (1996).

[18] The transformation of the dimensionless Eq. (1) into dimensional units is through $\Delta n(I) = -\Delta n_0/(1 + I)$. (ξ, η) coordinates are scaled by $\frac{\lambda}{2\pi}(\frac{n}{2\Delta n_0})^{1/2}$, and ζ is scaled by $(\frac{\lambda}{2\pi} \frac{n}{\Delta n_0})$. Typically, as in our experiments, $\Delta n_0/n$ is of the order of 2×10^{-4} for 10 μm FWHM solitons at $\lambda = 0.5$ μm. Note, that Eq. (1) is not integrable, so some power could escape from the soliton to radiation modes. This may lead to nonstationary propagation. In our simulations, power escape is small so there is no observable change in the soliton shape up to distances in excess of 30 diffraction lengths.

[19] M. Segev, G. C. Valley, B. Crosignani, P. DiPorto, and A. Yariv, Phys. Rev. Lett. **73**, 3211 (1994); D. N. Christodoulides and M. I. Carvalho, J. Opt. Soc. Am. B **12**, 1628 (1995).

[20] M. Shih, M. Segev, G. C. Valley, G. Salamo, B. Crosignani, and P. DiPorto, Electron. Lett. **31**, 826 (1995).

[21] A. Stepken *et al.,* Phys. Rev. Lett. **82**, 540 (1999).

[22] P. Ohberg and L. Santos, Phys. Rev. Lett. **86**, 2918 (2001); T. Busch and J. R. Anglin, *ibid.* **84**, 2298 (2000).

[23] S. Burger *et al.,* Phys. Rev. Lett. **83**, 5198 (1999); J. Denschlag *et al.,* Science **287**, 97 (2000).